Basic Study on Thrust Control Using Frequency Separation in Variable Pitch Propeller Mechanisms for Response and Efficiency Improvement of Drones

Yuto Naoki* Student Member, Kentaro Yokota* Student Member
Sakahisa Nagai* Member, Hiroshi Fujimoto* Senior Member

Recently, small multi-rotor drones have become popular. Conventional drones have simplicity with a fixed pitch angle of the propeller. Now, attempts to use drones for industrial purposes are currently underway, and in particular, large drones and flying mobilities are attracting attention. Variable pitch propellers are being considered and researched for such applications that require more advanced performance. Variable pitch propellers can achieve higher responsiveness than those controlled by rotational speed, but efficiency deteriorates when only the pitch angle is changed. In this study, we propose a method to improve the power consumption in the steady-state while achieving high responsiveness in the transient state. Both the pitch angle and the rotational speed are controlled using frequency separation to achieve the high responsiveness. The operation point in the steady-state is determined to minimize the power consumption or to achieve the high thrust. The effectiveness of the proposed method is verified by simulations and experiments.

Keywords: Drone, variable pitch propeller, thrust control, transient response, power optimization

1. Introduction

1.1 Recent drones and variable pitch propeller In recent years, the use of small unmanned aerial vehicles (after this, referred to as "drones"), mainly multi-rotor helicopter types, has been spreading rapidly. In particular, there is an increasing number of attempts to use drones for industrial purposes. In inspection and surveying, they are used for maintenance, inspection, and monitoring of bridges, power lines, etc. In addition, they have been used for dangerous manned tasks such as radiation dosimetry and volcanic gas measurement [2].

One of the factors that have made the multi-rotor type mainstream and widespread is the simplicity. Unlike the single-rotor type, the multi-rotor type has several propellers of whoes pitch are fixed and only the rotational speed are controlled. Instead, the multiple rotors are controlled independently to achieve stable flight despite the simplicity [2].

However, the fixed pitch propeller itself has a low degree of freedom due to the absence of a pitch angle change mechanism, which limits the performance. Also, in the future, drones are expected to be used in large vehicles such as flying cars and in industrial applications, which will require more sophisticated control. Therefore, the application of variable pitch propellers to drones, which can change the pitch angle, the angle between the propeller blade chord and the rotation plane, is being studied to improve the characteristics of the drones by taking advantage of the high degree of freedom.

Variable pitch propellers themselves have been used in propeller-driven aircraft and helicopters. Our group has also researched on the application of variable pitch propellers in electric aircraft (EA). The research conducted in the past includes power consumption minimization control by optimizing pitch angle and rotational speed [3], and regenerative energy optimization control [4].

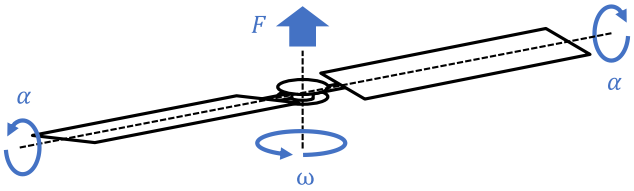

Fig. 1. Variable pitch propeller

1.2 Purpose of this study The following three points are mainly pointed out as the advantages of applying variable pitch propellers to drones in the previous studies.

- High responsiveness to achieve stable control [5]
- Reduction of power consumption [6]
- Suppression of noise and vibration [7] [8]

In addition, there are researches on the application of reversible thrust generation to special airframe shapes. [10] [9]

Among the above, the issues of responsiveness and power consumption are critical because they are greatly aggravated when aircraft become larger. In this respect, the application of the variable pitch propellers is a great advantage. The problem of the power consumption is also an issue in EA and the reduction of motor weight is researched. [11] For drones, the power used for hovering is larger and becomes more important. In addition, the responsiveness to respond to disturbances is required higher level for drones because they hold

* The University of Tokyo, 5-1-5, Kashiwanoha, Kashiwa, Chiba, 227-8561 Japan

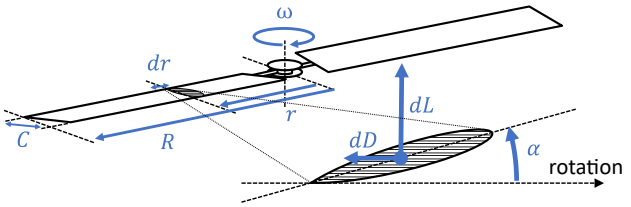

Fig. 2. Forces acting on wing element

their attitudes and position only by the thrust of the propeller.

In a previous study that focused on the response of the variable pitch propellers, it was pointed out that controlling the propeller pitch angle only dominantly improved the response of the attitude control compared to the conventional control based on only the rotational speed [5]. The effect on the responsiveness is particularly severe when the rotor diameter increases. However, this control method deteriorates efficiency. On the other hand, it has been analytically pointed out that the power efficiency can be optimized based on the model of the variable pitch propeller. [6]

This paper focuses on the precise control of the thrust force. The proposed method controls both the pitch angle and the rotational speed to achieve high responsiveness and reduce power consumption. The controller includes a frequency separation technique in order to utilize the actuator's characteristics efficiently.

2. Drone Propeller Dynamics and Model

The force generated by the propeller is explained by the blade element theory, which considers the force acting on a small portion of the blade surrounded by an arbitrary radius r and $r + \mathrm{d}r$. Fig. 2 shows forces actiong on the propeller blade element.

The differential lift $\mathrm{d}L$ and differential drag $\mathrm{d}D$ acting on the wing element are calculated as

$$\mathrm{d}L = \frac{1}{2}\rho(r\omega)^2 C_L C \mathrm{d}r \quad \cdots\cdots (1)$$

$$\mathrm{d}D = \frac{1}{2}\rho(r\omega)^2 C_D C \mathrm{d}r \quad \cdots\cdots (2)$$

where ω is ratational speed, ρ is air density, C is chord length, and C_L and C_D are constants of lift and drag respectively.

In the case of drones, the thrust and counter-torque generated by the entire propeller are equal to the sum of the lift L and drag D acting on the propeller blades, because the aircraft's airspeed V is almost zero in near-hovering flight conditions. Thus these forces are calculated as (3) and (4) by integrating (1) and (2) over radius r and multiplying by the number of blades b.

$$F = bL = \frac{b}{2}\rho\omega^2 \int_0^R C_L C r^2 \mathrm{d}r \quad \cdots\cdots (3)$$

$$Q = bD = \frac{b}{2}\rho\omega^2 \int_0^R C_D C r^2 \mathrm{d}r \quad \cdots\cdots (4)$$

The lift and drag coefficients C_L and C_D are dimensionless coefficients that depend on the aerodynamic settings of the propeller and the air around the propeller. These coefficients can be represented by first- and second-order functions for the propeller pitch angle α respectively. These models are shown in (5) and (6).

$$C_L = a_{L1}\alpha + a_{L0} \quad \cdots\cdots (5)$$

$$C_D = a_{D2}\alpha^2 + a_{D1}\alpha + a_{D0} \quad \cdots\cdots (6)$$

From these equations, the thrust and counter torque generated by the propeller calculated by (3) and (4) are rewritten as product of a coefficient that varies with the angle and a term that depends on the rotational speed. Therefore, the following equations can be derived.

$$F = (b_{F1}\alpha + b_{F0})\,\omega^2 \quad \cdots\cdots (7)$$

$$Q = \left(b_{Q2}\alpha^2 + b_{Q1}\alpha + b_{Q0}\right)\omega^2 \quad \cdots\cdots (8)$$

The equation of motion of the electrical motor is

$$T - Q = J_\omega \frac{\mathrm{d}\omega}{\mathrm{d}t} + B_\omega\omega + T_C, \quad \cdots\cdots (9)$$

where J_ω is inertia motor of the motor and propeller, B_ω is viscosity coefficient of motor and T_C is coulomb friction.

At this time, the input to the propeller is

$$\begin{aligned} P &= \omega T \\ &= \left(b_{Q2}\alpha^2 + b_{Q1}\alpha + b_{Q0}\right)\omega^3 \\ &\quad + B_\omega\omega^2 + \left(J_\omega \frac{\mathrm{d}\omega}{\mathrm{d}t} + T_C\right)\omega. \end{aligned} \quad \cdots\cdots (10)$$

Thus the power consumption also depends on the rotational speed and pitch angle.

3. Proposal of Thrust Control by Frequency Separation for Variable Pitch Propellers

3.1 Frequency-Separated Thrust Feedforward controller The method of thrust control using frequency separation consists of an internal pitch angle and rotational speed controller and a thrust controller that distributes the respective command values. In this research, the feedforward thrust controller was designed to investigate the basic effectiveness of frequency separation control for the variable pitch propeller. The whole block diagram of the proposed controller is shown in Fig. 3. The contents are explained in the following subsections.

3.1.1 Pitch angle and rotational speed controller The pitch angle and rotational speed used to control the thrust are controlled as a first-order system. Pitch angle α is controlled as a first-order system around the aerodynamic center of the propeller blade by the dynamics of the motor.

The rotational speed controller consists of a proportional controller with feedforward compensation by a model of the disturbance torque to the motor and feedback compensation by a disturbance observer. By using these compensator, the plant is nominalized and interference is not need to be considered. By this controller, the system can be assumed as a first-order system. The current control is sufficiently fast in the inner.

The respective transfer functions are shown in (11).

$$\frac{\Delta\alpha}{\Delta\alpha^*} = \frac{1}{\tau_\alpha s + 1}, \quad \frac{\Delta\omega}{\Delta\omega^*} = \frac{1}{\tau_\omega s + 1} \quad \cdots\cdots (11)$$

where τ_α and τ_ω are response time of each controller.

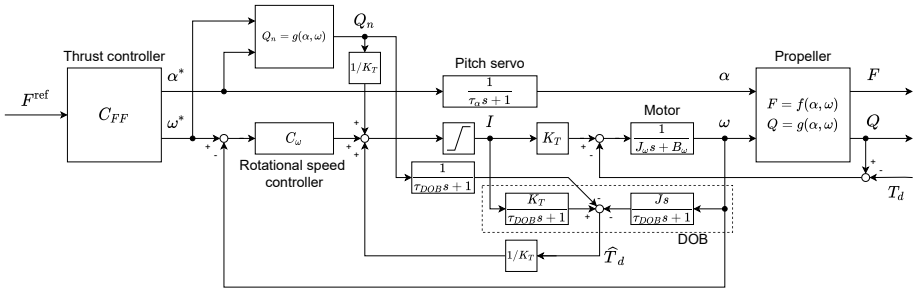

Fig. 3. Block diagram of frequency separation feedforward control

3.1.2 Thrust controller The thrust controller allocates from the thrust command value to the respective command values of pitch angle and rotational speed.

Firstly, the thrust model shown in (7) is linearized about the operating conditions α_0 and ω_0.

$$\begin{aligned}\Delta F &= b_{F1}\omega_0^2\Delta\alpha + 2\omega_0(b_{F1}\alpha + b_{F0})\Delta\omega \\ &= a\Delta\alpha + b\Delta\omega \quad \cdots\cdots\cdots\cdots\cdots\cdots\cdots\cdots \quad (12)\end{aligned}$$

The first-order delay in the control from the command values of the pitch angle and rotational speed α^*, ω^* to the actual values α, ω shown in (11) are considered.

$$\Delta F = \frac{a}{\tau_\alpha s + 1}\Delta\alpha^* + \frac{b}{\tau_\omega s + 1}\Delta\omega^* \quad \cdots\cdots\cdots\cdots\cdots\cdots \quad (13)$$

Considering this equation, a simple feedforward controller from the command value of the thrust ΔF^{ref} to each actuator command value of the rotational speed and pitch angle is designed to set the control of thrust as a first-order system with the desired time constant τ as shown in (14). The controllers designed are shown in (15) and (16).

$$\Delta F = \frac{1}{\tau s + 1}\Delta F^{\mathrm{ref}} \quad \cdots\cdots\cdots\cdots\cdots\cdots\cdots\cdots \quad (14)$$

$$\Delta\alpha^* = \frac{\tau_\alpha s + 1}{a} \cdot x \cdot \frac{1}{\tau s + 1}\Delta F^{\mathrm{ref}} \quad \cdots\cdots\cdots\cdots\cdots\cdots \quad (15)$$

$$\Delta\omega^* = \frac{\tau_\omega s + 1}{b} \cdot y \cdot \frac{1}{\tau s + 1}\Delta F^{\mathrm{ref}} \quad \cdots\cdots\cdots\cdots\cdots\cdots \quad (16)$$

where, steady-state values are determined by the control distribution x and y.

3.1.3 Allocation design In the proposal, the allocation of the command values are designed considering the following two conditions.

(i) In the transient response, the propeller pitch is used for the high-frequency component and the rotational speed is used for the low-frequency component.

(ii) In the steady-state, it transitions to the desired combination of the rotational speed and pitch angle. (Rotational speed and pitch angle of the transition destination can be determined by other factors such as power consumption.)

By determining the desired rotational speed $\Delta\omega^{\mathrm{ref}}$ and pitch angle $\Delta\alpha^{\mathrm{ref}}$ in the final steady-state, the final values k_α, k_ω of the allocation terms x, y, shown in (15) and (16), can be calculated as

$$k_\alpha = \frac{a}{\Delta F^{\mathrm{ref}}}\Delta\alpha^{\mathrm{ref}} \quad \cdots\cdots\cdots\cdots\cdots\cdots\cdots\cdots \quad (17)$$

$$k_\omega = \frac{b}{\Delta F^{\mathrm{ref}}}\Delta\omega^{\mathrm{ref}}. \quad \cdots\cdots\cdots\cdots\cdots\cdots\cdots\cdots \quad (18)$$

By calculating these equations, the condition (ii) is taken into account.

As the premise of the equations, the desired combination of rotational speed and pitch angle in the steady-state is determined to satisfy the equation (19) to avoid steady-state error.

$$F + \Delta F^{\mathrm{ref}} = \left\{b_1\left(\alpha + \Delta\alpha^{\mathrm{ref}}\right) + b_0\right\}\left(\omega + \Delta\omega^{\mathrm{ref}}\right)^2 \quad \cdot (19)$$

Furthermore, condition 1 of the transient response can be taken into account by applying a low-pass filter (LPF) with a time constant of τ_1 to the command value on the slow-response speed side and adding the remaining high-pass filter (HPF) portion to the pitch angle. As a result, the command value allocation is

$$x = k_\alpha + k_\omega\frac{\tau_1 s}{\tau_1 s + 1} \quad \cdots\cdots\cdots\cdots\cdots\cdots\cdots\cdots \quad (20)$$

$$y = k_\omega\frac{1}{\tau_1 s + 1}. \quad \cdots\cdots\cdots\cdots\cdots\cdots\cdots\cdots \quad (21)$$

By substituting these into the equation (15) and (16), the thrust command can be separated to command values of rotational speed and pitch angle since $x + y \approx 1$, and achieve designing the thrust response by feedforward control and transition to the desired operating state.

3.1.4 Optimization of propeller output power One of the advantages of being able to control both the rotational speed and pitch angle is that the thrust can be generated by a good combination of them in the steady-state. A possible method of calculating the combination of the rotational speed and pitch angle is to make it conditional on the reduction of power consumption. A method of controlling the rotational speed and pitch angle to optimize the power consumption by the propeller in steady-state can be calculated as follows. Here, the power consumption of the pitch servo is considered to be smaller enough than main motor.

Assuming that the frictional term in (10) is sufficiently small, the power consumption by the propeller is highly dependent on the counter-torque by the propeller.

$$P = \omega Q = \left(b_{Q2}\alpha^2 + b_{Q1}\alpha + b_{Q0}\right)\omega^3 \quad \cdots\cdots\cdots\cdots \quad (22)$$

When operating in certain thrust, from (7), the rotational speed can be expressed using the pitch angle as follows:

$$\omega = \sqrt{\frac{F}{b_{F1}\alpha + b_{F0}}} \quad \cdots\cdots\cdots\cdots\cdots\cdots\cdots\cdots (23)$$

From (22) and (23), the power consumption is

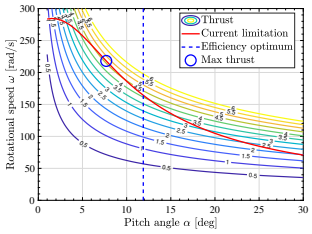

Fig. 4. Thrust contour and limit based on the model

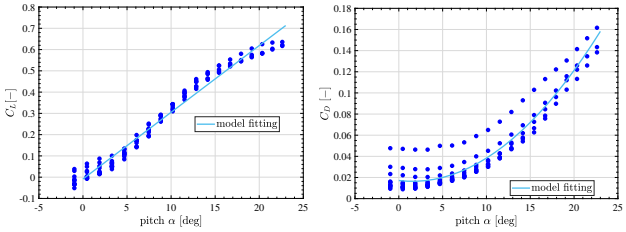

(a) Lift coefficient (b) Drag coefficient

Fig. 5. (a) Relationship between pitch angle and lift coefficient (b) Relationship between pitch angle and Drag coefficient

$$P = \frac{\left(b_{Q2}\alpha^2 + b_{Q1}\alpha + b_{Q0}\right)}{\left(b_{F1}\alpha + b_{F0}\right)^{\frac{3}{2}}} F^{\frac{3}{2}}. \quad \cdots\cdots\cdots\cdots\cdots \quad (24)$$

Thus, α which minimizes P is

$$\begin{aligned}\alpha =& \frac{1}{2b_{D2}b_{L1}}\Bigg[-\left(4b_{D2}b_{L0} - b_{D1}b_{L1}\right) \\ &+ \Big\{\left(4b_{D2}b_{L0} - b_{D1}b_{L1}\right)^2 \\ &- 4b_{D2}b_{L1}\left(2b_{D1}b_{L0} - 3b_{L1}b_{D0}\right)\Big\}^{\frac{1}{2}}\Bigg] \quad \cdots\cdots\cdots \quad (25)\end{aligned}$$

and is constant regardless of F. This means that in order to reduce power consumption while prioritizing responsiveness, the strategy of using the pitch angle only in transient response and then gradually converting it to the rotational speed and returning to the optimum pitch angle is effective as long as the model of (22) is assumed.

3.1.5 Thrust range expansion control On the other hand, in the method of operating at the optimum pitch angle in the steady-state, the motor current limit determines the rotational speed limit, which determines the upper limit of the thrust that can be output.

Fig. 4 shows example of the constant thrust line, current limitation and power optimum line calculated by (7), (8) and (25). As shown in Fig. 4, the output thrust increases by lowering the pitch angle and increasing the rotational speed while the maximum torque value Q_{max} is constant. Thus, when the current value reaches the maximum value, the method of changing both pitch angle and rotational speed becomes effective for the final steady-state.

4. Simulation

A simulation is conducted to verify the proposed method.

The simulation model uses the parameter of propeller of DTS 300. The lift and drag coefficients of this propeller are shown in Fig.5.

The motor parameters are the values of the motor used in the experiment setup, and a limit of 10 A is set for the current value.

Table 1. Lift and Drag coefficients

Parameter	Value
b_{F1}	1.32×10^{-5}
b_{F0}	-3.61×10^{-6}
b_{Q2}	4.20×10^{-8}
b_{Q1}	-1.32×10^{-7}
b_{Q0}	2.34×10^{-6}

Table 2. Step response simulation conditions

Parameter	Value
Operating rotational speed ω_0	800 rpm
Operating pitch angle α_0	11.8°
Operating thrust F_0	1.2 N
Thrust reference ΔF^{ref}	1 N
Time constant of rotational speed control τ_ω	0.27 s
Time constant of pitch angle control τ_α	0.04 s
Time constant of frequency separation filter τ_α	0.1 s

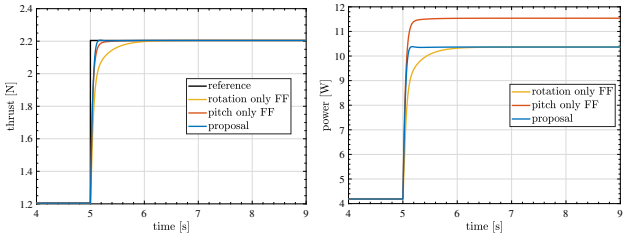

(a) Thrust (b) Power

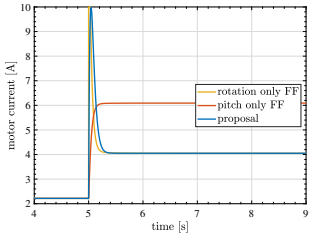

(c) Motor current

Fig. 6. Simulation result

4.1 Feedforward control simulation The step response of the thrust dimention only using the feedforward controller are verified in the simulation. The conditions are shown in Table 2.

The result of the simulation is shown in Fig. 6. Fig. 6(a) is the step response of the thrust, Fig. 6(b) is the power which consumed in the propeller, and Fig. 6(c) is the motor current. As shown in Fig. 6(a), the 3% settling time of the feedforward thrust control using only the rotational speed was about 1s slower than that of the feedforward control using only the pitch angle and the proposed method. As shown in Fig. 6(c), in the feedforward control using only the rotational speed, the motor current reached the limits of 6 A. The reason is that excessive current value was required in order to increase the response from the original time response. This current saturation causes deterioration of the step response. The thrust control by pitch angle only and the proposed method did not reach the current limit and followed the designed thrust.

On the other hand, one of the problems is the error in transient response caused by linearization. In the theory of the proposed method, the thrust is approximated by a first order system by considering $x + y \approx 1$, in (15) and (16). However,

Table 3. Range expansion simulation conditions

Parameter	Value
Operating rotational speed ω_0	1000 rpm
Operating pitch angle α_0	11.8°
Operating thrust F_0	1.7 N
Thrust reference ΔF^{ref}	2.5 N
Pitch angle reference $\Delta\alpha^{\mathrm{ref}}$	−3°

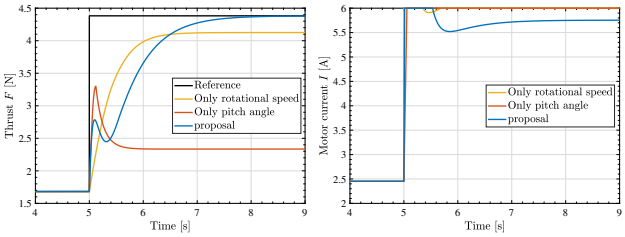

(a) Thrust (b) Motor current

Fig. 7. Range expansion simulation result

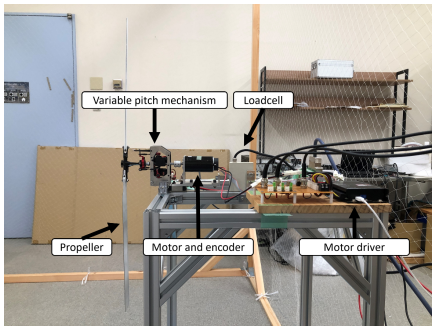

Fig. 8. Experimental setup

in reality, there is an error in the linearization, and this error occurs because the allocation is calculated backward from the rotational speed and pitch angle that have the desired thrust in the steady-state so that there is no steady-state error. In order to reduce the error, feedback control can be added to reduce the error, and this is a future work.

4.2 Thrust range expansion simulation The effect of the thrust range expansion control was also verified in the simulation. The conditions are shown in Table 3. The final value of the pitch angle was set as −3°.

The result of simulation is shown in Fig. 7. As shown in Fig. 7(a), the control only by pitch angle and the control only by rotational speed with efficiency optimum pitch angle did not achieve the reference and remain error. On the other hand proposed method achieved the final value. In the proposed method, the response of the thrust once decreases when the current reached the limit as shown in Fig. 7(b). However, this effect is temporary and, after this, rise time was the same as that of the control only by the rotational speed.

5. Experiment

5.1 Setup Fig. 8 shows a picture of the experimental setup. The experimental unit consists of a linear guide, a load cell, a motor, an encoder and a variable pitch propeller. The load cell measures F and the encoder measures ω in rad s^{-1}.

Before the experiment, J_ω, B_ω and T_C are identified. The identification method was based on Yokota (2020) [12].

The viscosity coefficient B_ω and coulomb friction T_C of the motor were measured by the motor torque in the no-load test.

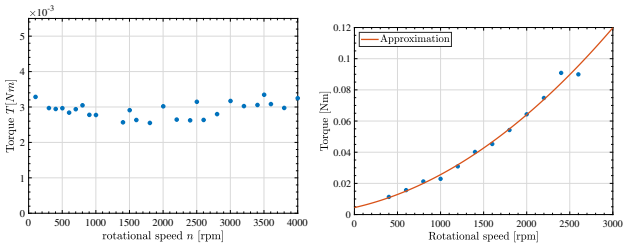

(a) $\omega - T$ relation of motor without propeller (b) $\omega - T$ relation of motor with propeller

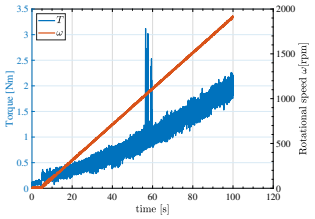

(c) ramp response with propeller

Fig. 9. Motor-Propeller parameters identification

Table 4. Parameters

Parameter	Value
Inertia moment of propeller J_ω	4.0×10^{-4} kgm^2
Viscosity coefficient of motor B_ω	4.6×10^{-6} N m s rad^{-1}
Coulomb friction of motor T_C	2.4×10^{-3} N m
Torque constant K_T	30.2×10^{-3} N m A^{-1}
Max. continuous current $I_{\max}$	6 A

The result is shown in Fig. 9(a).

Next, from the torque values measured when obtaining Fig. 5(b), the relation between the rotational speed and torque at constant speed when the pitch angle is 0.45° was measured. This relationship is shown in Fig. 9(b).

At this time, as shown in (8), the counter-torque is proportional to the square of the rotational speed. The relation between counter torque and torque is

$$T = Q + B\omega + T_C. \quad \cdots\cdots\cdots\cdots\cdots\cdots\cdots\cdots (26)$$

Thus a quadratic approximation can be applied to the relation between rotational speed and torque in Fig. 9(b).

Finally, the torque of the motor under the constant acceleration command was measured. The result is shown in Fig. 9(c). The torque is

$$T = J\frac{\mathrm{d}\omega}{\mathrm{d}t} + Q + B\omega + T_C. \quad \cdots\cdots\cdots\cdots\cdots\cdots (27)$$

The inertia is calculated by subtracting the result of the Fig. 9(b) from Fig. 9(c).

The values of and the motor parameters obtained in the preliminary experiments and for the motor are shown in Table 4.

5.2 Feedforward control experiment The experimental results of the feedforward thrust step command of the conventional and proposed methods are shown in Fig. 10. All of these results were processed by a zero-phase digital filter, which is 10 times faster than the pitch angle control.

Fig. 10(a) shows the thrust step response. The thrust reference command is 1 N step at t =10 s. As shown in the result, the rise time of the thrust controlled by rotational speed only was 0.4 s. On the other hand, the rise time of thrust controlled

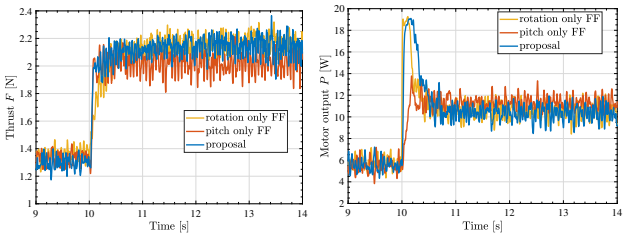

(a) Thrust F (b) Power P

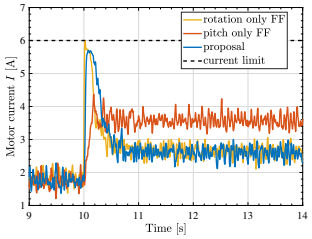

(c) Motor current I

Fig. 10. 1 N thrust step experiment results

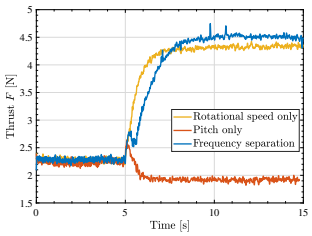

Fig. 11. Range expansion experiment results

by pitch angle only and the proposed method are both 0.1 s. Thus the proposed method achieved the same responsiveness as the control by pitch angle which is four times faster than thrust control using only the rotational speed. This difference in the result is caused by the current limit which can be confirmed in Fig. 10(c).

Also, Fig. 10(b) shows the power output of the motor calculated from the current and the rotational speed. In steady-state, it can be seen that the average power is 10.8 W for the proposal, whereas 11.2 W for thrust control using pitch angle only. Thus the proposal achieved the improvement of power consumption in the steady-state.

5.3 Thrust range expansion experiment The experimental results of thrust range expansion control are shown in Fig. 11. The operating point of the maximum thrust was determined from a map measured in advance.

As shown in the result, the proposed method achieved 0.2 N larger thrust than conventional methods. Thus the effect of the thrust range expansion control was confirmed. However, the reverse response during transient was also verified. The allocation method when the current reached the limit needs improvement and this is a future work.

6. Conclusion

The use of the variable pitch propellers is considered a solution to the demand for more advanced and efficient control of drones in industrial applications. This paper proposed a method to control propeller thrust using two types of actuators: rotational speed and pitch angle, which have a different response time. In the proposed method, a fast thrust transient response can be achieved by using the rotational speed in the slow frequency range and the pitch angle in the fast frequency range and the power consumption during the steady-state can be improved by repositioning the pitch angle. The results of simulation and experiments show the improvement of the transient response and steady-state power consumption.

The range of thrust can also be extended by appropriately allocating the pitch angle and rotational speed in the region of the power limitation of the motor.

As future works, we plan to reduce the steady-state error, which was a problem in the experiment. By adding feedback control or using thrust map, the steady-state error can be reduced.

Acknowledgment

The authors would like to thank Prof. O. Shimizu for his valuable advice and technical assistance with the experiments. This research was partly supported by the Ministry of Education, Culture, Sports. Science, and Technology grant (Grant Number JP18H03768).

References

(1) UM. R. Mogili and B. B. V. L. Deepak, "Review on application of drone systems in precision agriculture," *Procedia computer science 133*, pp.502–509, 2018.

(2) K. Nonami, "Drone technology, cutting-edge drone business, and future prospects." *Journal of Robotics and Mechatronics* vol. 28, no. 3, pp. 262–272, 2016.

(3) N. Kobayashi, H. Fujimoto, Y. Hori, H. Kobayashi and A. Nishizawa, "A study of Range Extension Control System by Optimization of Motor Torque and Propeller Pitch Angle for Electric Airplane" *Technical Meeting on Industrial Instrumentation and Control (IIC)*. IEEJ, pp.31–36, 2013.

(4) Y. Xiang, H. Fujimoto, Y. Hori, Y. Watanabe, and K. Suzuki, " Proposal of Regeneration Power Control System by Optimization of Propeller Pitch Angle and Revolution Speed for Electric Airplanes, " in *IEE* of Japan Technical Meeting Record, no. MEC-15-49, pp. 121–126, 2015.

(5) M. Cutler and J. P. How, "Analysis and control of a variable-pitch quadrotor for agile flight," *Journal of Dynamic Systems, Measurement, and Control*, vol. 137, no. 10, 2015, pp. 101002–101016.

(6) V. M. Arellano-Quintana, E. A. Merchán-Cruz and A. Franchi, "A Novel Experimental Model and a Drag-Optimal Allocation Method for Variable-Pitch Propellers in Multirotors," *IEEE Access*, vol. 6, pp. 68155–68168, 2018, doi: 10.1109/ACCESS.2018.2879636.

(7) Y. Tanabe, T. Aoyama, M. Sugiura, H. Sugawara, S. Sunada, K. Yonezawa and H. Tokutake, "Aerodynamic Interactions Between Rotors on a Multi-Copter Drone," in *JAXA Special Publication: Proceedings of the 48th Fluid Dynamics Conference / the 34th Aerospace Numerical Simulation Symposium*, pp. 141–146, 2016.

(8) R. Tanaka, Y. Tanabe, S. Sunada, K. Yonezawa and H. Tokutake, "Study of Influence of Phase-angle Differences on Aerodynamic Interactions between Rotors," in *JAXA Special Publication: Proceedings of the 49th Fluid Dynamics Conference / the 35th Aerospace Numerical Simulation Symposium*, pp. 53–59, 2017.

(9) K. Kawasaki, M. Zhao, K. Okada and M. Inaba, "MUWA: Multi-field universal wheel for air-land vehicle with quad variable-pitch propellers," 2013 IEEE/RSJ International Conference on Intelligent Robots and Systems, 2013, pp. 1880–1885, doi: 10.1109/IROS.2013.6696605.

(10) S. Komizunai, M. Uraoka and A. Konno, "Development and Thrust Response Evaluation of a Variable Pitch Propeller Quad Tilt-rotor Drone," *Transactions of the Society of Instrument and Control Engineers* vol. 56, no. 5, pp.310–316, 2020.

(11) K. Takishima and K. Sakai, "Design Method for Ultralightweight Motor Using Magnetic Resonance Coupling and its Characteristics," *IEEJ Journal of Industry Applications*, Article ID 21003160, [Advance publication] Released August 06, 2021.

(12) K. Yokota, H. Fujimoto and Y. Hori, "Basic Study on Regenerative Air Brake Using Observer-based Thrust Control for Electric Airplane," in *2020 IEEE 16th International Workshop on Advanced Motion Control (AMC)*. IEEE, pp. 34–39, 2020.